JOURNAL OF APPLIED PHYSICS VOLUME 95, NUMBER 11 1 JUNE 2004

The high-explosive channel effect: Influence of boundary layers on the precursor shock wave in air

Vincent Tanguay and Andrew J. Higgins
Department of Mechanical Engineering, McGill University, Montreal, Canada H3A 2K6

(Received 24 October 2003; accepted 4 March 2004)

The high-explosive channel effect is investigated to study the dynamics of the precursor shock wave in air when there is no coupling of the precursor with the detonation. This is achieved experimentally by using Detasheet in square channels. It is found that the precursor shock wave initially propagates at the velocity dictated by one-dimensional gasdynamics, but then slows down from its theoretical velocity. In fact, the precursor eventually (after hundreds of channel diameters) reaches a terminal velocity equal to the detonation velocity. It is found that boundary layers are responsible for this effect: shocked gas leaks past the detonation products through the boundary layer and, as a result, the precursor shock slows down. This phenomenon is modeled analytically and the results are found to agree well with experiments. [DOI: 10.1063/1.1715134]

I. INTRODUCTION

When a detonation propagates in an explosive layer that only partially fills a channel, the rapidly expanding detonation products can act as a piston and drive a precursor shock wave in the air gap (between the explosive layer and the channel confinement). This is illustrated in Fig. 1 and is typically referred to as the channel effect.

If the detonation has a constant velocity and the detonation products form an impermeable piston, then the Rankine-Hugoniot relations dictate the precursor shock wave velocity, which should be constant and 10% to 20% greater than the detonation velocity. Indeed, this has been observed experimentally by Woodhead,[1] Woodhead and Titman,[2] Ahrens,[3] and Johansson and Persson[4] in internal channels (channels in which the air gap is completely surrounded by explosive). However, in external channels (where the explosive is surrounded by an air gap), the result is different: the precursor shock wave, after an initial transient, slows down to the detonation velocity (as observed by Johansson and Persson,[4] Johansson *et al.*,[5] and Goldbinder and Tysevič[6]). In other words, the detonation and the precursor shock wave both travel at the same velocity at a constant distance apart. In this case, the impermeable piston assumption is clearly not valid, as air must be leaking through the detonation products interface. However, the mechanism of air leakage has yet to be determined.

Moreover, it is known that the cross-sectional area ratio of explosive to air gap influences the channel effect. In the limit of a large air gap, the explosive is effectively unconfined and no precursor shock wave can be observed, i.e., there is simply a decaying blast wave that cannot overtake the detonation. At the other extreme, as the air gap is made very small, the explosive becomes completely confined, and again, no precursor shock wave can run ahead of the detonation. However, there is a range between these limits where the channel effect can be observed. It has been found by Sumiya *et al.*[7] that the optimal area ratio of explosive to air gap to produce the channel effect is approximately one to one (optimal meaning maximum precursor shock wave velocity and standoff and best agreement with theory for an impermeable piston). However, the understanding of this behavior is, at present, qualitative only.

In the same study,[7] it was found that wall roughness was also an important parameter. Indeed, when the walls of an external channel were lined with sandpaper, the precursor shock wave propagated at a lower velocity (with a shorter standoff). In fact, with sufficient wall roughness, the precursor shock wave velocity was reduced to the detonation velocity. Once again, the description of this phenomenon is only qualitative.

As the precursor shock wave runs ahead of the detonation, it may precondition the unreacted explosive and can influence the detonation propagation. Depending on the type of explosive, the detonation propagation can couple with the precursor shock wave through various mechanisms. The insensitive heterogeneous explosives used in commercial blasting, for example, require voids for detonation propagation. A precursor shock wave precompresses the explosive and eliminates the voids and can cause the detonation to fail. This coupling mechanism, called "dead pressing," is clearly an undesirable effect but can be avoided by using sleeves as obstacles in the bore hole.[4]

If the explosive is porous but sensitive enough not to require voids for detonation propagation, then the detonation can accelerate.[2–4,8] The greater detonation velocity is simply due to the greater initial density of the precompressed explosive. This coupling mechanism will be treated in a future publication.

Finally, if the explosive is very sensitive, the precursor shock wave could initiate an oblique detonation in the explosive layer. The precursor shock wave would be driven at a greater velocity due to the greater apparent velocity of the detonation. This positive feedback mechanism can lead to extremely high propagation velocities, several times the detonation velocity of the initial explosive. This has been

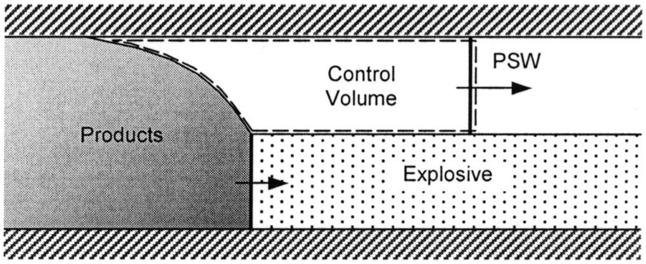

FIG. 1. Sketch of the channel effect.

observed by Bakirov and Mitrofanov,[9] and Mitrofanov.[10] This coupling mechanism will also be treated in a future publication.

In the present investigation, the channel effect is studied under conditions in which there is no coupling between the detonation and the precursor shock wave. The goal is to understand and model the mechanism governing the dynamics of the precursor shock wave in the simplest configuration where the detonation velocity is constant.

II. EXPERIMENTAL DETAILS

For the detonation to be independent of the precursor shock wave (PSW), the explosive must have the following characteristics. It must be at (or near) the theoretical maximum density (TMD) so that no significant precompression occurs, and it must be insensitive enough not to be initiated by the PSW. The explosive used in this investigation was Detasheet, a plastic bonded pentaerythritol tetranitrate (PETN) sheet. It is a secondary explosive with a density of approximately 1.51 g/cc.

Square cross-section channels were built from strips of 3 mm thick gray polyvinyl chloride (PVC) sheets. Figure 2 shows the configuration of a typical channel. Channels of internal side, $w=2h=6$, 10, 12, and 16 mm were investigated. The channel lengths varied from 70 to 200 cm. In all cases, the Detasheet explosive filled the bottom half of the channel. Thus, in all cases, the area ratio of explosive to air gap was maintained at one to one. The explosive ran the entire length of the channel and extended out of the channel by approximately 10 cm, where a detonator was attached for initiation. All experiments were conducted in ambient air.

These charges were instrumented with self-shorting twisted wire pairs (SSTWP) underneath the Detasheet to detect the time of arrival of the detonation. Piezoelectric shock pins (Dynasen Model CA-1135) were mounted on top of the channel, flush with the inside of the air gap. As well, self-shorting brass foil contact gauges were used to determine the time of arrival of the PSW. The spacing between time-of-arrival probes varied depending on the channel dimensions.

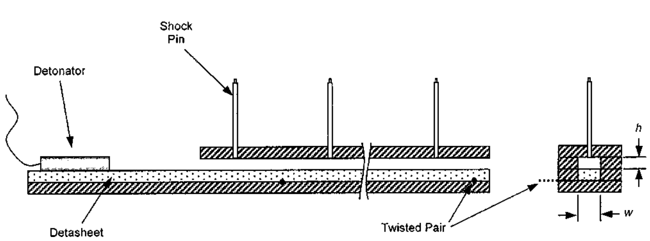

FIG. 2. Schematic of a typical channel and diagnostics.

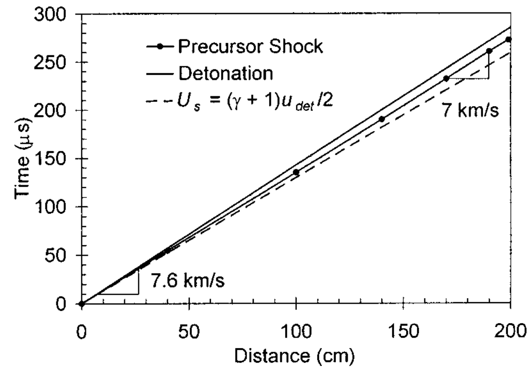

FIG. 3. Trajectories of the detonation and the precursor shock wave in a $w=16$ mm channel.

III. RESULTS

First, unconfined Detasheet was detonated. The velocity of detonation (VOD) was measured by the use of SSTWPs. The VOD was very reproducible and determined to be 7.05 ± 0.05 km/s.

The Detasheet was then detonated in a channel with an air gap. The trajectories of the detonation and the PSW of a typical experiment ($w=16$ mm) are shown in Fig. 3. The VOD of Detasheet was unchanged and constant at approximately 7 km/s. This implies that the detonation was unaffected by the PSW. The contact gauges and shock pins detected the presence of the PSW in the air gap, ahead of the detonation. Initially, the PSW propagated significantly faster than the detonation: approximately 7.6 km/s. However, as the shock wave propagated in the channel, it decelerated until its propagation velocity was the same as that of the detonation. This is clear from Fig. 3 where, initially, the two trajectories diverge but eventually become nearly parallel. This means that a terminal configuration is reached, where the PSW propagates at a constant distance of 7–8 cm ahead of the detonation, in this case.

This is also illustrated in Fig. 4 where the standoff (distance between the PSW and the detonation) is plotted as a function of the detonation position along the channel. This

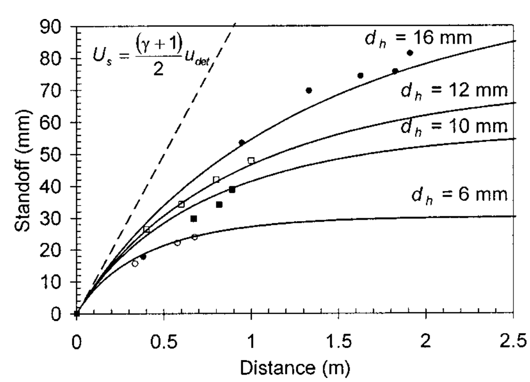

FIG. 4. Standoff (distance between the PSW and the detonation) as a function of propagation distance in channels with $w=6$, 10, 12, and 16 mm.

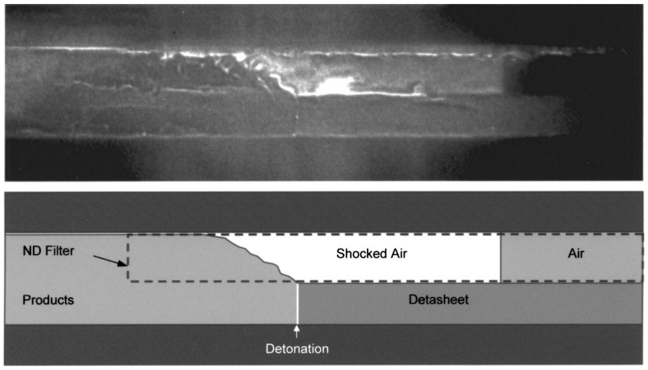

FIG. 5. High-speed photograph of the channel effect in a $w=6$ mm channel (top) and interpretation (bottom).

figure includes the data for 6, 10, 12, and 16 mm channels. For any given channel, the standoff increases rapidly at first but then asymptotes a terminal value. This figure also illustrates the effect of channel diameter. Larger standoffs are observed in larger channels after a given distance of propagation. Also, larger terminal standoffs are obtained in larger diameter channels.

Figure 5 is a high-speed photograph of the detonation propagating from left to right taken with a DiCam-PRO, an image intensified charge-coupled device (CCD) camera. The exposure duration was 20 ns. The channel was backlit with a COOKEScope Model 125 xenon flash. For this reason, the PVC confinement, the Detasheet layer, and the detonation products are opaque to the back lighting and appear dark on the photograph. The shocked air behind the PSW appears bright on the photograph because its temperature is very high (almost 10 000 K according to NASA's equilibrium code CEA (Ref. 11)). In fact, the gas is brighter than it appears in the photograph because a 5% neutral density filter was placed in front of the air gap (the location of the filter is indicated in Fig. 5 by the dashed line). The photograph also shows the detonation in the Detasheet as a very narrow bright vertical line.

A. Impermeable piston assumption

The "pistonlike" motion of the expanding detonation products drives the PSW down the channel. The piston velocity is constant and equal to the detonation velocity of 7 km/s. If this is the case, the shock wave velocity should also be constant and dictated by the following Rankine-Hugoniot relation:

$$\frac{u_p}{U_s}=\frac{2}{\gamma+1}\left[1-\frac{1}{M^2}\right], \tag{1}$$

where U_s is the shock velocity, u_p is the piston velocity (or particle velocity), M is the shock Mach number, and γ is the ratio of specific heats of the gas. Note that even though the piston is oblique, the PSW is perfectly normal to the channel axis, justifying the use of one-dimensional Rankine-Hugoniot relations. For strong shock waves, the above can be simplified to

$$U_s \approx \frac{\gamma+1}{2} u_p . \tag{2}$$

For such strong shock waves ($M \approx 20$), γ cannot be taken to be 1.4. However, an equilibrium code such as NASA's CEA (Ref. 11) can be used to predict a better estimate. This results in a value of $\gamma \approx 1.2$. The equilibrium code can directly predict the $U_s - u_p$ relationship. For a particle velocity of 7 km/s, CEA predicts a shock velocity of 7.65 km/s. This is in good agreement with the measured velocity of the PSW at early times ($t < 50\ \mu$s). The trajectory of this constant velocity shock wave is illustrated in Figs. 3 and 4 as dashed lines.

B. Mechanisms for mass leakage

Consider a control volume bounded by the PSW, the detonation products interface (the piston) and the channel walls (see Fig. 1). The above results are based on the assumption that the interface of the detonation products is impermeable, forming a constant velocity piston driving the PSW. However, because the shock wave slows down and eventually reaches the piston velocity, the above assumption must clearly be invalid. In other words, gas must be leaking out of the control volume. In fact, when the velocity of the PSW is equal to the detonation (piston) velocity, the mass flux out of the control volume must be equal to the mass flux into the control volume. There are three possible explanations for this, which will be discussed in the following sections.

1. Confinement yielding

The first possibility is that the PVC confinement may be yielding because of the high pressure of the shocked gas. If it were so, gas could be leaving the control volume through the opening created in the channel, or mass could be accumulating in the expanding control volume. However, a simple order-of-magnitude analysis reveals that on the time scale of interest (a few microseconds), the channel will only move by less than 10 μm under the force exerted by the shocked gas (at approximately 350 atm). Since this dimension is much smaller than the typical channel dimension, the channel can be considered to be essentially rigid. Finally, the high-speed photograph of Fig. 5 shows clearly that on the time scale of interest the channel confinement is rigid.

2. Permeable piston

It is also possible that the detonation products do not expand all the way to the upper wall. For example, if the height of the air gap was much larger than the thickness of explosive, it is obvious that the detonation products would not expand all the way to the wall. They would only drive an oblique shock or a bow shock, which would never run ahead of the detonation. In the present experiment, a precursor shock does run ahead and so the combustion products do presumably expand all the way to the wall. Note, however, that it is possible to have a precursor shock even if the products do not expand all the way to the upper confinement. If they come sufficiently close, they can form a throat and choke the air flow in the channel. In this case, there would still be a precursor shock. However, its velocity should still

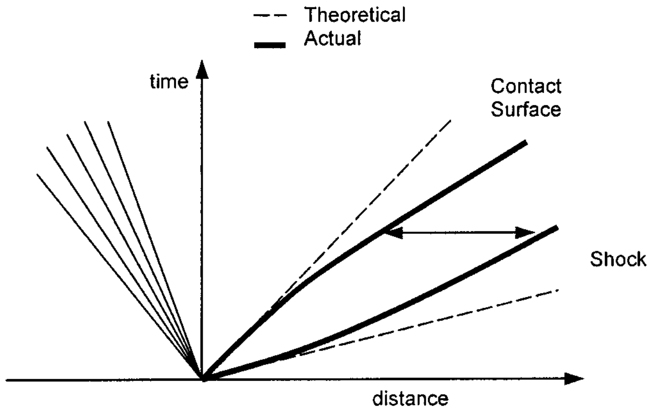

FIG. 6. Wave diagram of events in a real shock tube; the shock wave slows down and reaches a terminal velocity.

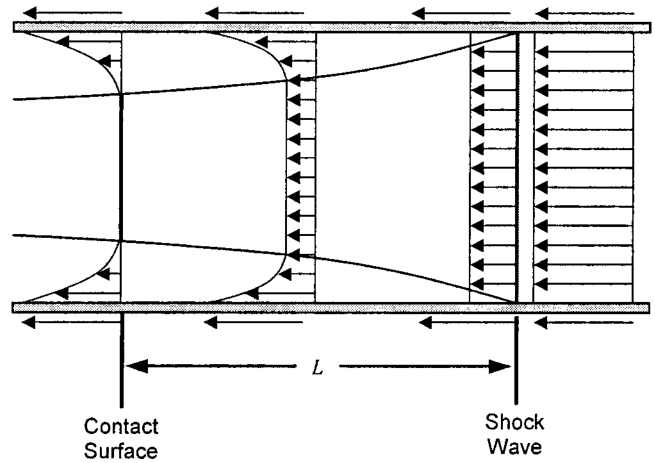

FIG. 7. In a shock tube, behind the shock wave, boundary layers plow gas through contact surface, which results in a terminal shock velocity. This phenomenon is analogous to the present experiment.

be constant, but lower than in the impermeable piston case. This phenomenon was described and analyzed by Mitrofanov.[10]

In the high-speed photograph of Fig. 5, it can be seen that the detonation products do expand all the way to the upper wall. Furthermore, the interface between the shocked air and the detonation products may not be impermeable. It is possible for this interface to be turbulent, and therefore, shocked gas may be entrained into the detonation products and leak out of the control volume. In any case, this effect would be very difficult to quantify or to demonstrate.

3. Boundary layers

Finally, gas could be leaking across the interface through boundary layers on the channel walls. In fact, it is well known that boundary layers cause a similar effect in shock tubes. Figure 6 is a sketch of an $x-t$ diagram representing the events in a shock tube. Theory predicts that both the contact surface (interface) and the shock wave should move at constant velocities (straight lines on the $x-t$ diagram). However, in practice, the contact surface speeds up and the shock wave slows down. This continues until a terminal configuration is reached, where the shock wave and the contact surface move with the same velocity (a constant distance apart). This is analogous to what is observed in the present experiment. In shock tubes, this phenomenon is due to boundary layers, and it is illustrated in Fig. 7.

Ahead of the shock, the gas and the wall both have the same velocity toward the control volume (in the shock frame of reference). However, upon crossing the shock, the gas is slowed down. At this point, there is a velocity difference between the wall and the gas. Therefore, because of the viscosity of the gas, a boundary layer begins to grow. Near the wall, the gas is moving toward the contact surface faster than in the free stream. At the contact surface, the gas in the boundary layer is able to exit the control volume. Essentially, the wall, through viscous forces, plows gas through the contact surface.

Mirels[12] proposed a model to predict the distance between the shock and the contact surface. This can be done easily by equating the mass flux into the control volume to the mass flux out of the control volume. The mass flux out of the control volume is a function of the boundary layer displacement thickness, which in turn is a function of the distance between the shock wave and the contact surface. This model can easily be adapted to the present experiment. It can also be extended to predict not only the steady-state distance but also the transient development.

IV. BOUNDARY LAYER MODEL

First, consider the control volume bounded by the shock, the contact surface (in this case the detonation products interface), and the channel walls [see Fig. 8(a)]. Also, denote the velocity of the shock wave as U_s, the velocity of the detonation (contact surface) as u_{det}, and the particle velocity behind the shock as u_p [all these velocities are in the lab frame of reference; see Fig. 8(b)]. The subscripts *o*, *s*, and *w* refer to initial conditions, post shock conditions, and conditions at the wall, respectively. Assume that the perfect gas law applies and that the temperature of the wall is constant

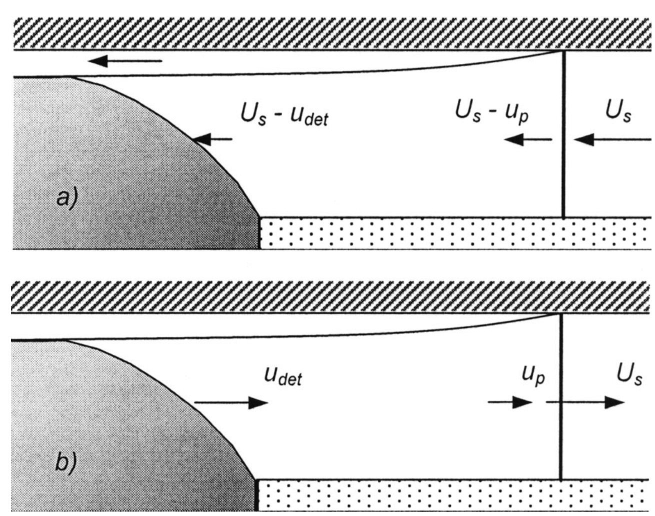

FIG. 8. Control volume in the (a) steady (shock) reference frame and (b) unsteady (lab) reference frame.

$(T_w = T_o)$. This assumption is valid because on the time scale of interest (a few microseconds), there is no time for the wall to heat up.

Mirels states that at steady state, the net mass flux into the control volume is equal to zero. However, more generally, we can say that the rate of mass accumulation in the control volume is equal to the net mass flux:

$$\frac{d}{dt} m_{cv}(t) = \dot{m}_{in} - \dot{m}_{out}, \tag{3}$$

where $m_{cv}(t)$ is the mass of the control volume at any time t and $\dot{m}_{in}$ and $\dot{m}_{out}$ are mass flux in and out of the control volume, respectively. Assuming that the density is constant and uniform inside the control volume and approximating the shape of the control volume as a rectangle, the mass of the control volume can be expressed in terms of its length $L(t)$:

$$m_{cv}(t) = A\rho_s L(t), \tag{4}$$

where A is the cross-sectional area of the of the air gap and ρ_s is the postshock density. From Rankine-Hugoniot relations, the density ratio across a strong shock wave is a constant and approximated by Eq. (5):

$$\frac{\rho_s}{\rho_o} = \frac{\gamma+1}{\gamma-1}. \tag{5}$$

Therefore, differentiating the mass of the control volume [Eq. (4)] with respect to time, we get

$$\frac{d}{dt} m_{cv}(t) = \left(\frac{\gamma+1}{\gamma-1}\right) A\rho_o \frac{d}{dt} L(t). \tag{6}$$

The mass flux into and out of the control volume can be expressed as

$$\dot{m}_{in} = A\rho_o U_s, \tag{7}$$

$$\dot{m}_{out} = p\,\delta_i \rho_w U_s, \tag{8}$$

where p is the perimeter of the air gap (along which there are boundary layers), δ_i is the boundary layer displacement thickness at the interface, and ρ_w is the density of the gas at the wall. It is assumed here [in Eq. (8)] that the boundary layer displacement thickness is small compared to the dimensions of the channel. Whether or not this is a valid assumption will be discussed later. Mirels used the Blasius relation for the boundary layer displacement thickness:

$$\delta_i \equiv \beta L^{1-n} \left[\frac{\nu_w}{u_p}\right]^n, \tag{9}$$

where β is a constant, ν_w is the kinematic viscosity of the gas at the wall, u_p is the particle velocity of the gas behind the shock (with respect to the wall), and $n = 1/2$ for laminar and $n = 1/5$ for turbulent boundary layers. Note as well that the shock velocity is related to the detonation (piston) velocity through Eq. (10):

$$U_s = u_{\mathrm{det}} + \frac{dL}{dt}. \tag{10}$$

Define the hydraulic diameter of the channel as

$$d_h \equiv \frac{4A}{p}. \tag{11}$$

Now, because of the thermal boundary layer, the temperature of the gas at the wall will be the same as the temperature of the wall. Furthermore, we can assume that the temperature of the wall will be constant (before and after the shock), because on the time scale of interest, the wall has infinite heat capacity compared to the gas. Therefore, we can use the perfect gas law and write

$$\rho_w = \frac{P_s}{P_o} \rho_o, \tag{12}$$

since

$$T_w = T_o. \tag{13}$$

The pressure ratio across the shock wave is given by the following Rankine-Hugoniot relation (simplified for strong shock waves):

$$\frac{P_s}{P_o} = \frac{2\gamma M^2}{\gamma+1}. \tag{14}$$

Finally, substituting Eqs. (4)–(14) into Eq. (3) and rearranging, one obtains

$$\left(\frac{2}{\gamma-1}\right)\frac{dL}{dt} = u_{\mathrm{det}} - \frac{4\beta}{d_h} \nu_o^n \left(\frac{2}{\gamma+1}\right)^{1-2n} \times \left[\frac{\gamma L}{c_o^2}\left(u_{\mathrm{det}} + \frac{dL}{dt}\right)^3\right]^{1-n}, \tag{15}$$

which is an implicit, nonlinear, ordinary differential equation in $L(t)$. The above equation can easily be nondimensionalized. Let

$$l = \frac{L}{d_h}, \quad X = \frac{x}{d_h}, \quad T = \frac{u_{\mathrm{det}} t}{d_h}, \quad M_{\mathrm{det}} = \frac{u_{\mathrm{det}}}{c_o},$$

and

$$\mathrm{Re} = \frac{u_{\mathrm{det}} d_h}{\nu_o}. \tag{16}$$

After substitution, Eq. (15) becomes

$$\left(\frac{2}{\gamma-1}\right)\frac{dl}{dT} = 1 - \frac{4\beta}{\mathrm{Re}^n}\left(\frac{2}{\gamma+1}\right)^{1-2n} \times \left[\gamma M_{\mathrm{det}}^2 l \left(1 + \frac{dl}{dT}\right)^3\right]^{1-n}. \tag{17}$$

The dependence on diameter (or Reynolds number) can be eliminated by making the following substitutions:

$$\mathcal{L} = \gamma M_{\mathrm{det}}^2 l \left[\left(\frac{2}{\gamma+1}\right)^{1-2n} \frac{4\beta}{\mathrm{Re}^n}\right]^{1/1-n},$$

$$\chi = \gamma M_{\mathrm{det}}^2 X \left[\left(\frac{2}{\gamma+1}\right)^{1-2n} \frac{4\beta}{\mathrm{Re}^n}\right]^{1/1-n},$$

and

TABLE I. Model parameters.

Parameter	Value
u_{det} (m/s)	7000
β	0.01
c_o (m/s)	350
ν_o (m^2/s)	1.569×10^{-4}
γ	1.19

$$\tau=\gamma M_{\mathrm{det}}^2 T\left[\left(\frac{2}{\gamma+1}\right)^{1-2n}\frac{4\beta}{\mathrm{Re}^n}\right]^{1/1-n}. \tag{18}$$

Then, Eq. (17) becomes

$$\left(\frac{2}{\gamma-1}\right)\frac{d\mathcal{L}}{d\tau}=1-\left[\mathcal{L}\left(1+\frac{d\mathcal{L}}{d\tau}\right)^3\right]^{1-n}, \tag{19}$$

which is indeed independent of diameter (or Reynolds number).

A. Laminar or turbulent

Until this point, it has not yet been determined if the boundary layer is laminar or turbulent. This can be achieved by computing the Reynolds number based on L_∞, Re_{L_∞}, which is defined as follows:

$$\mathrm{Re}_{L_\infty}\equiv\frac{u_p L_\infty}{\nu_w}. \tag{20}$$

A numerical value for Re_{L_∞} can be obtained by substituting numerical values from Table I. For a hydraulic diameter of say 10 mm, the result is $\mathrm{Re}_{L_\infty,turbulent}\approx 10^{10}$. We can now compare Re_{L_∞} with a transition Reynolds number Re_t. According to Mirels, the transition from laminar to turbulent occurs in the following range: $0.5\leqslant \mathrm{Re}_t\times 10^{-6}\leqslant 4$. This is valid for shock Mach numbers in the range $1\leqslant M\leqslant 9$. The transition Reynolds number increases beyond this range of Mach numbers because of the stabilizing effects of the low wall temperatures. However, only limited data is available for stronger shock waves. Nevertheless, the computed Reynolds number is four orders of magnitude higher than the upper limit of the transition Reynolds number. This strongly suggests that the boundary layer is indeed turbulent.

B. Steady-state solution

Even though it is rather straightforward to integrate Eqs. (15) or (19) numerically, it can be insightful to consider the steady-state solution since it will be possible to obtain an analytical solution.

As time evolves ($t\rightarrow\infty$) the distance between the PSW and the detonation will approach a constant maximum value. This implies that L will approach a constant. The terminal standoff L_∞ can be obtained by setting dL/dt equal to zero in Eq. (15) and solving for L. This gives

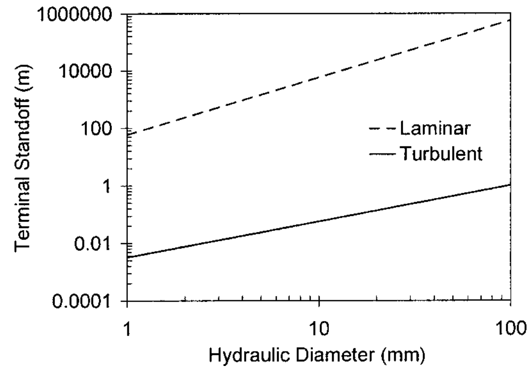

FIG. 9. Terminal standoff as a function of channel hydraulic diameter.

$$L_\infty=\left(\frac{d_h}{4\beta}\right)^{1/1-n}\left(\frac{\gamma+1}{2}\right)^{2n-1/n-1}\times\frac{c_o^2}{\gamma}(\nu_o)^{n/n-1}(u_{\mathrm{det}})^{3n-2/1-n}, \tag{21}$$

where the parameters that govern the terminal standoff can be identified as the hydraulic diameter, the properties of the gas (ratio of specific heats, sound speed, and viscosity), and the detonation velocity. We can substitute in the above $n=1/5$ for turbulent boundary layers:

$$L_{\infty,\mathrm{turbulent}}=\left(\frac{d_h}{4\beta}\right)^{5/4}\left(\frac{\gamma+1}{2}\right)^{3/4}\frac{c_o^2}{\gamma\nu_o^{1/4}u_{\mathrm{det}}^{7/4}}. \tag{22}$$

The turbulent terminal standoff is plotted in Fig. 9 as a function of hydraulic diameter for air. The terminal standoff increases with an increasing hydraulic diameter: the PSW runs further ahead.

C. Boundary layer thickness

In the derivation of the above model, it was assumed that the boundary layer was thin compared to the dimensions of the channel. This assumption can now be verified using Eq. (9) to compute the boundary layer displacement thickness at L_∞. Substituting Eq. (21) into Eq. (9) to eliminate L_∞, one obtains

$$\frac{\delta_{L_\infty}}{d_h}=\left[\frac{(\gamma+1)c_o^2}{8\gamma u_{\mathrm{det}}^2}\right]=5.73\times 10^{-4} \tag{23}$$

and so indeed, the boundary layer displacement thickness is much smaller (three to four orders of magnitude) than the dimensions of the channel. Therefore, it is clear that this assumption is valid. It is interesting to note that this ratio is independent of the type of boundary layers: laminar or turbulent.

D. Full unsteady solution

To obtain the full unsteady solution, Eq. (15) must be integrated. This differential equation is nonlinear and implicit in dL/dt, and therefore, very difficult to integrate analytically. However, it can readily be integrated numerically with an appropriate initial condition. The initial condition is

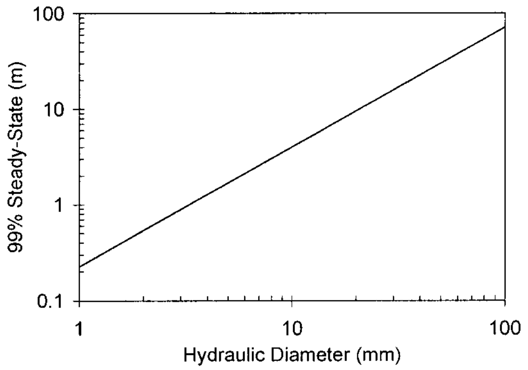

FIG. 10. Distance of propagation required to reach 99% of the terminal standoff for turbulent boundary layers.

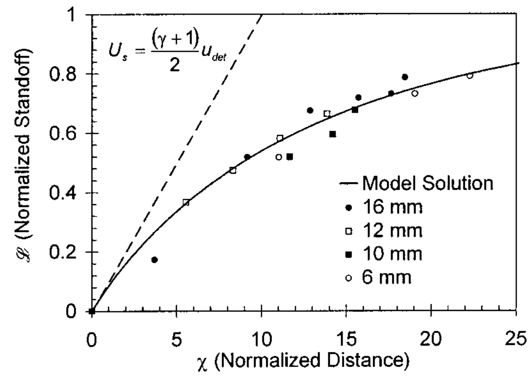

FIG. 11. Normalized standoff as a function of normalized distance of propagation (model and experimental results for 6, 10, 12, and 16 mm hydraulic diameter channels).

that the distance between the PSW and the detonation must be zero. As the detonation enters the channel, there is no shock wave, but it forms at this point and begins to move ahead.

The solution is plotted for different hydraulic diameters in Fig. 4, and agrees well with the experimental data. Note the dependence on diameter: the larger the diameter the greater the terminal standoff, but it also means a longer time (or distance of propagation) to approach the steady-state value. This is shown in Fig. 10, where the distance of propagation to reach 99% of the maximum value is plotted versus hydraulic diameter.

One also notes that for all diameters, the initial slope is the same, which means that the initial velocity of the precursor is the same. This was to be expected. Initially, because the standoff is very small, the boundary layer at the interface is very thin. In the limit, it has zero thickness. This means there is no mass leakage and that the interface acts as an impermeable piston. In this case, the problem is independent of geometry and Eq. (2) dictates the velocity of the shock. We can also see this from Eq. (15) when L is set equal to zero, the equation reduces to

$$\frac{dL}{dt}=\frac{(\gamma-1)}{2}u_{\mathrm{det}}. \tag{24}$$

Adding u_{det} to both sides of the above we obtain

$$U_s=u_{\mathrm{det}}+\frac{dL}{dt}=\frac{(\gamma+1)}{2}u_{\mathrm{det}}, \tag{25}$$

which is same as Eq. (2).

Figure 11 shows the solution to Eq. (19) (Eq. (15) normalized). The family of solutions of Fig. 4 now collapses onto a single curve. The experimental data has also been normalized and included on Fig. 11. Again the agreement is very good.

One should note that the hydraulic diameter of the channels has been taken as

$$d_h=\frac{4wh}{w+2h}, \tag{26}$$

where w and h are the width and the height of the air gap, respectively. Note that the denominator is not the entire perimeter of the channel but includes only three sides. It is anticipated that the boundary layers forming on those three sides only will cause leakage through the contact surface. Because of the very high detonation pressure, it is unlikely that the boundary layer on the explosive surface will successfully penetrate the detonation products interface.

V. CONCLUSIONS

The dynamics of the precursor shock wave were isolated from interaction with the explosive. Indeed with Detasheet, no coupling was observed between the detonation and the PSW. This allowed the identification and modeling of the appropriate governing mechanism: boundary layers.

The present results strongly suggest that boundary layers play an important role in the channel effect. In fact, in the present experiments, boundary layers seem to be the main mechanism that governs the dynamics of the channel effect. It is due to boundary layers on the channel walls that the precursor shock wave slows down from its theoretical velocity. They also give rise to a maximum standoff that can be achieved by the PSW.

In light of these results, previous experiments become much clearer. For example, Johansson and Persson[4] noted a significant difference between internal and external channels. In internal channels the PSWs propagate at constant velocities, well predicted by the assumption of an impermeable piston. However, external channels have precursor shock waves that rapidly decelerate and reach a terminal configuration. The difference is due to the fact that internal channels are not exposed to any walls; they are completely bounded by explosive and therefore boundary layers play an insignificant role. In the present experiments, the air gaps are exposed to confinement walls and can therefore be considered as external channels. These are affected by boundary layers, which form on confinement walls.

Furthermore, Sumiya *et al.*[7] noted a decrease in precursor shock velocity with increasing wall roughness. Again, this is consistent with the present conclusion: rougher walls mean thicker boundary layers and a decrease in shock velocity.

Finally, note that the effect of boundary layers can be minimized. The model derived above showed a clear dependence on the diameter of the channel. By making the diameter larger, the cross-sectional area to perimeter ratio increases, which minimizes the effect of boundary layers.

ACKNOWLEDGMENT

The authors would like to thank Geneviève Savoie for her help in conducting experiments. This project was supported by Fonds québécois de la recherche sur la nature et les technologies (FQRNT) Grant 2001-NC-66936

[1] D. W. Woodhead, Nature (London) **160**, 644 (1947).
[2] D. W. Woodhead and H. Titman, Explosivstoffe **13**, 113 (1965); **13**, 141 (1965).
[3] H. Ahrens, Explosivstoffe **13**, 124 (1965).
[4] C. H. Johansson and A. Persson, *Detonics of High-explosives* (Academic Press, London, 1970).
[5] C. H. Johansson, H. L. Selberg, and A. Persson (unpublished).
[6] A. I. Goldbinder and V. F. Tysevič̂, in *Theory of Explosives*, edited by K. K. Andreev (Vychaja Chola, Moscow, 1967).
[7] F. Sumiya, K. Tokita, M. Nakano, Y. Ogata, Y. Wada, M. Seto, K. Katsuyama, and S. Itoh, J. Mater. Process. Technol. **85**, 25 (1999).
[8] F. H. G. McCaffrey, U.S. Patent No. 4,402,270 (3 September 1983).
[9] I. T. Bakirov and V. V. Mitrofanov, Sov. Phys. Dokl. **21**, 704 (1976) [Dokl. Akad. Nauk. SSSR, **231**, 1315 (1976)].
[10] V. V. Mitrofanov, Acta Astron. **3**, 995 (1976).
[11] S. Gordon and B. J. McBride, computer code CEA, NASA, 1994.
[12] H. Mirels, AIAA J. **2**, 84 (1964).